Title

Enhancer lncRNA LOC730338 limits the innate immune response against lymphoma cells, inhibiting ADAR2-dependent alternative transcription.

Luciano Cascione [1,2], Francesca Guidetti [1], Sunandini Ramnarayanan [3,4,5], Andrea Rinaldi [1], Filippo Spriano [1], Alex Zadro [1,6], Chiara Tarantelli [1], Nicolas Munz [1], Alberto J. Arribas [1,2], Rory Johnson [4], Francesco Bertoni [1,7*], Sara Napoli [1*]

[1] Institute of Oncology Research, Faculty of Biomedical Sciences, USI, Bellinzona, Switzerland; [2] SIB Swiss Institute of Bioinformatics, Lausanne, Switzerland; [3] School of Biology and Environmental Science, University College Dublin, Dublin, D04 V1W8, Ireland; [4] Conway Institute for Biomolecular and Biomedical Research, University College Dublin, Ireland; [5]The SFI Centre for Research Training in Genomics Data Science, Dublin, Ireland; [6] Laboratories for Translational Research, Ente Ospedaliero Cantonale, Bellinzona, Switzerland; [7]Oncology Institute of Southern Switzerland, Ente Ospedaliero Cantonale, Bellinzona, Switzerland.

***Co-corresponding authors:**

-Dr Sara Napoli, Institute of Oncology Research, via Francesco Chiesa 5, 6500 Bellinzona, Switzerland.

e-mail: sara.napoli@ior.usi.ch.

-Prof. Francesco Bertoni, Institute of Oncology Research, via Francesco Chiesa 5, 6500 Bellinzona, Switzerland e-mail: francesco.bertoni@ior.usi.ch.

Abstract (150 words)

Chronic antigenic stimulation is central to marginal zone lymphoma (MZL) development. While the pharmacological inhibition of the B-cell receptor (BCR) signaling is initially effective, secondary resistance frequently develops. We conducted a CRISPR interference (CRISPRi) screen investigating enhancer-associated long non-coding RNAs (elncRNAs) in MZL cells to identify transcripts crucial to shape their dependence on BCR pathway activation. We identified LOC730338, an elncRNA associated with A-to-I RNA editing, which we renamed ADARreg. Silencing ADARreg re-sensitized tumor cells to BCR pathway inhibition by modulating ADAR2 nuclear translocation and altering intronic RNA editing. The process preferentially affected genes that enhance immune responses, such as STING, IRF3, and p65. ADARreg knockdown also increased lymphoma cell sensitivity to NK cell-mediated cytotoxicity. Our results indicate that targeting elncRNAs like ADARreg represents a potential strategy to overcome drug resistance in lymphoma, also opening new therapeutic opportunities for immunotherapy.

Marginal zone Lymphoma (MZL) derives from MZ B cells under chronic inflammation and prolonged B cell receptor (BCR) activation from persistent infections or autoimmune diseases [1]. A hallmark of MZL is the interaction of tumor cells with the microenvironment, a complex network of various cell types, including T cells, which communicate through soluble factors like cytokines and chemokines. BCR signaling plays a key role in shaping these interactions and activating downstream pathways like NF-kB [2], to sustain lymphoma growth [3]. Indeed, the pharmacological inhibition of BCR signaling, particularly through Bruton's tyrosine kinase (BTK) inhibition with the first-in-class ibrutinib and newer agents, is an effective therapeutic option for MZL patients as well as for other lymphoid neoplasms [4-6]. However, resistance frequently develops [7, 8], and, in lymphoma cells, it is frequently sustained by , in lymphoma cells, it is frequently sustained by epigenetic reprogramming [9-12].

Non-coding RNAs (ncRNAs), particularly enhancer-associated long non-coding RNAs (elncRNAs), play key roles in regulating gene expression [13]. The elncRNAs are transcribed from enhancer regions and act as transcription regulators in a tissue-specific and developmentally regulated manner [14]. They derive from super-enhancers (SEs), large clusters of highly acetylated enhancers bound by transcription factors, regulating key differentiation genes [15, 16]. ElncRNAs often stabilize protein complexes *in cis* but can also acquire *in trans* activity, affecting both nuclear and cytoplasmatic additional functions [17, 18].

Here, we aimed to identify elncRNAs modulating the transcriptional reprogramming in ibrutinib-resistant splenic MZL (SMZL) via a screen based on the Clustered Regularly Interspaced Short Palindromic Repeats Interference (CRISPRi) technology. Among the identified transcripts, the lncRNA LOC730338 (AC011294.3/ENSG00000233539) emerged due to its previously identified role in regulating A-to-I RNA editing in B cells [19]. We show that it likely acts as a negative regulator of ADARB1 and, to a lesser extent, ADAR, genes that encode the adenosine deaminases ADAR2 and ADAR1, respectively [19]. Based on this, we renamed it ADARreg and demonstrated its role in modulating the sensitivity to ibrutinib and also for an immune-suppressive capacity.

RESULTS

Acquired ibrutinib-resistance in SMZL cells is associated with changes in super-enhancer activation

The VL51 cell line, which originated from a patient with a SMZL [20], was cultured for up to nine months under increasing doses of ibrutinib, leading to secondary resistance to BTK inhibitors and other BCR pathway-targeting drugs, such as the PI3K inhibitors idelalisib, duvelisib and copanlisib [21]. *In vitro* BCR stimulation revealed that, in ibrutinib-resistant cells, NF-κB signaling showed reduced BCR dependency compared to parental cells (Fig.S1A).

To study the epigenetic remodeling of BCR-blocked cells, we investigated the enhancer activity in ibrutinib-resistant VL51, using ChIP-sequencing to profile histone modifications (H3K27ac, H3K4me1, and H3K4me3). We identified 33,264 H3K27ac peaks: 20,950 common, 2,830 unique to parental cells, and 541 to resistant cells (Fig.1A, Table S1). Bona fide enhancers were defined by the presence of H3K4me1 and the absence of H3K4me3. Comparing ibrutinib-resistant cells to their parental counterparts, we found that resistant cells lost 1,329 enhancers and gained 144 new ones (Fig.1A, B). Taking advantage of the RNAseq from parental and derivative cells, we examined the genes within 40 kb of these differentially

activated enhancers. Loss of enhancers was linked to the downregulation of key genes, including CDKN2A, CDKN2B, and MAP3K14, with the most notable decrease observed in NLRP4, a pattern-recognition receptor (PRR) involved in immune activation (Fig.1C, left) [22]. A few genes near newly activated enhancers were significantly upregulated in resistant cells (Fig.1C, right). This suggested that additional non-coding transcripts might be associated with these enhancer gains.

Identification of elncRNAs associated with ibrutinib resistance

SEs, densely bound by transcription factors and highly acetylated, regulate crucial genes and are the main source of elncRNAs. Using the ROSE algorithm [23], we identified 1,345 SEs from H3K27Ac ChIP-Seq data. (Fig.S1B). To determine how many SEs were associated with elncRNA production, we reconstructed the transcriptomes of parental and ibrutinib-resistant VL51 cells using total RNA-Seq profiling. We included a VL51 derivative resistant to PI3Kδ inhibitors [11] to expand our analysis beyond ibrutinib-resistance. By analyzing ribosomal RNA-depleted libraries, we detected polyadenylated and non-polyadenylated transcripts and identified novel and known transcripts associated with SEs (Fig.S1B). We defined elncRNAs as any transcript detectable within an active SE in either parental or resistant cells. We assigned a transcription start site (TSS) based on the FANTOM project CAGE dataset [24] (Fig S1B). We excluded transcripts annotated as protein-coding genes but included antisense or sense intronic transcripts. We identified 427 elncRNAs, including 74 novel transcripts not listed in GENCODE (Fig.S1B). Of these, 13% (45 elncRNAs) were lost, and 9% (30 elncRNAs) were gained in the ibrutinib-resistant cells (Fig.S1A, Table S2).

Functional screening of elncRNAs linked to BCR blockade

To identify elncRNAs associated with BCR blockade, we performed a genome-wide CRISPRi screen in both parental and ibrutinib-resistant cells (Fig.2A). We designed a custom library of paired guide RNAs (pgRNAs) that targeted 255 annotated elncRNAs and 57 novel ones (Fig.2B). The library also included pgRNAs targeting 225 lincRNAs differentially expressed between parental and resistant cells, 68 essential genes as positive controls, and 33 non-expressed transcripts as negative controls. The whole library investigated 659 transcripts (Fig.2B, Table S2). The pgRNAs were designed to target regions within -300 to +300 base pairs around the TSSs by a defective Cas9 fused with the repressor ZIM3 (dCas9-KRAB-ZIM3) [25] (Fig.2A, S1C), allowing transcriptional repression without inducing DNA damage [25].

After elncRNA CRISPRi library infection (Fig.S1D), parental and resistant cells were treated with either ibrutinib or DMSO for two weeks (Fig.2C). We analyzed two replicates per condition at three time points (6, 10, and 14 days) compared to time 0 (Fig.2C). The effects of specific transcripts on cell survival and BCR dependency, assessed by ibrutinib sensitivity, were measured through pgRNAs enrichment overtime, represented by β score (Fig.2D, Table S3). Positive β values indicated that transcripts impaired proliferation or increased drug sensitivity, negative β values the opposite. The high β correlation for positive controls across replicates validated the robustness of our approach (Fig.S1E).

The β correlation for elncRNA targets was consistent, albeit higher in parental cells, possibly reflecting greater heterogeneity in the resistant population (Fig.S1F). Multi-dimensional scaling (MDS) plots showed lincRNA silencing differentiated parental from resistant cells, especially after 14 days (Fig.S1G). Similarly, elncRNA silencing discriminated resistant from parental cells starting as early as day 6 (Fig.2D). Notably, some elncRNAs affected resistant cell survival only with drug exposure (Fig.2D).

132 The distribution of β scores in parental and resistant cells exposed to ibrutinib showed concordance of
133 many transcripts modulating the drug response, especially among lincRNAs (Fig 2E, left). However, some
134 elncRNAs peculiarly affected ibrutinib efficacy in resistant or parental cells. Noteworthy, silencing
135 AC011294.3 (ADARreg) (FigS2A) and RP11-96H19.1 (lncPCED1b) (Fig.S2B) was sufficient to revert BCR
136 dependency in resistant cells (Fig 2E, right).

137 **ADARreg affects the sensitivity to ibrutinib**

138 To confirm ADARreg function, we transduced Ibrutinib-resistant VL51 cells with constructs expressing
139 mCherry and pgRNAs targeting the ADARreg TSS, and GFP-tagged dCas9ZIM3 (Fig.S2C). Dual fluorescent
140 markers tracked ADARreg knockdown (eRNA_kd) cells within mixed populations for a competitive assay.
141 We monitored double-positive cells over 10 days, comparing them to wild-type cells. The competition
142 assay confirmed the CRISPRi screening results. ADARreg knockdown cells were more sensitive to ibrutinib
143 than the wild-type and pgRNA-expressing cells, confirming transcriptional interference caused these
144 effects (Fig.S2C).

145 **lncPCED1b validation as regulator of ibrutinib response**

146 RP11-96H19.1 (ENSG00000257261), referred to as lncPCED1b due to its proximity to the *PCED1b* gene
147 (Fig.S2B), was identified in the CRISPRi screen as promoting ibrutinib sensitivity in Ibrutinib-resistant VL51
148 cells and, to a lesser extent, in parental cells (Fig.2E). Stable interference with lncPCED1b transcription in
149 both cell types reduced cell survival in resistant cells respect with control cells transduced with pgRNAs
150 targeting KLK12, a non-expressed gene in our model. (Fig.S2D).

151 After two weeks, double-positive cells were sorted and expanded to establish stable knockdown models.
152 We confirmed that ADARreg or lncPCED1b knockdown enhanced sensitivity to BTK inhibition in Ibrutinib-
153 resistant cells (Fig.S2E). However, parental cells with lncPCED1b knockdown did not retain the phenotype
154 (Fig.S2E).

155 **ADARreg silencing affects A-to-I editing in intronic regions**

156 Given ADARreg's potential role in regulating A-to-I RNA editing [19], we analyzed the transcriptional
157 variants between parental VL51 cells, Ibrutinib-resistant cells expressing KLK12 pgRNAs, and Ibrutinib-
158 resistant cells with stable knockdowns of ADARreg or lncPCED1b. Using the RED-ML algorithm, we
159 identified approximately 24,000 editing sites within Alu sequences and 13,000 outside them across all
160 experimental conditions (Table S4).

161 Focusing on sequence-specific editing sites found in at least three samples, we discovered that 66%
162 (n=1,857) occurred outside Alu sequences and 33% (n=952) within (Fig.3A, left). Differential editing
163 analysis identified 195 non-Alu and 86 Alu-specific editing sites in the resistant cells. Similar analyses
164 comparing ibrutinib-resistant cells with ADARreg knockdown (n=85 non-Alu; n=14 Alu) or lncPCED1b
165 knockdown (n=69 non-Alu; n=18 Alu) showed that elncRNA silencing primarily affected editing outside
166 Alu regions (Fig.3A, right).

167 We also examined the genomic distribution of editing sites. Approximately 30% occurred in the 3'UTR,
168 20% in exons (mostly synonymous variants), 15% as exonic missense variants, and 17% in introns (Fig.3B).
169 ADARreg and lncPCED1b knockdown notably affected the editing sites within introns (Fig.3B).

170 In Ibrutinib-resistant cells, intronic editing was largely lost compared to parental cells (Fig.3C, left).
171 ADARreg knockdown reversed this trend, increasing intronic editing in protein-coding genes while
172 decreasing in noncoding genes (Fig.3C, middle). Similarly, lncPCED1b knockdown also increased intronic
173 editing sites (Fig.3C, right). Many of the editing sites restored by ADARreg knockdown were initially
174 present in parental cells but lost in resistant cells (Fig.3D), and the differentially edited transcripts were
175 predominantly involved in immune and cancer-related pathways (Table S5).

176 **ADARreg affects the editing of ncRNAs involved in ibrutinib sensitivity**

177 Using the MEME tool, we identified a consensus sequence in the elncRNAs expressed in our model
178 (Fig.4A), complementary with a portion of the Alu element (Fig.4B, Table S6). This sequence is prone to
179 form a stable double-stranded RNA (dsRNA) structure (Fig.4C). When analyzing the full set of SEs active in
180 our model, no comparable consensus sequence with equal dsRNA-forming potential was identified
181 (Fig.4A, S3A). This suggested SE-transcribed regions were predisposed to editing. Indeed, several
182 elncRNAs and lincRNAs included in the CRISPRi screen were differentially edited in resistant compared to
183 parental cells (Fig.4D). Of particular interest, 37 editing sites showed significant differential editing in the
184 absence of ADARreg, most of which were more edited than the controls (Fig.4D). lncPCED1b (RP11-
185 96H19.1) was the third most edited ncRNA in ADARreg knockdown cells (Fig.4D). Remarkably, lncPCED1b
186 knockdown partially restored the parental editome in resistant cells (Fig.4E). Additionally, a subset of
187 differentially edited sites overlapped between lncPCED1b and ADARreg knockdown, suggesting that
188 lncPCED1b mediates A-to-I editing regulated by ADARreg (Fig.4F).

189 To further validate this, we analyzed parental cells with stable knockdowns of lncPCED1b or LINC00511, a
190 known oncogene not associated with RNA editing. Editing sites altered by LINC00511 knockdown were
191 less correlated with those involved in resistance than ADARreg knockdown (Fig.S3B-D). Notably,
192 lncPCED1b knockdown did not similarly affect the editome of parental cells, where ADARreg expression
193 was irrelevant for ibrutinib resistance (Fig.S3E). Furthermore, intronic editing events after lncPCED1b or
194 LINC00511 knockdown were less pronounced in parental cells than in resistant ones (Fig.S3F, G).

195 **ADARreg modulates BTK inhibition by regulating ADAR2 activity**

196 We tested ADARreg function in ibrutinib-resistant VL51 and Jeko1 cells. Jeko1, a mantle cell lymphoma
197 (MCL) line, expressed ADARreg and showed low sensitivity to ibrutinib. Stable ADARreg silencing in both
198 cell lines significantly increased their sensitivity to ibrutinib compared to cells expressing control KLK12-
199 pgRNAs (Fig.5 A, B, S4A).

200 To confirm that ADARreg *per se* contributed to drug resistance, we used antisense oligonucleotides to
201 degrade ADARreg in Jeko1 cells. Electroporation with Locked Nucleic Acids (LNAs) targeting ADARreg
202 reduced cell proliferation and increased sensitivity to ibrutinib (Fig.5C).

203 We further tested ADARreg's impact on drug sensitivity in HAIRM, an ibrutinib-sensitive cell line derived
204 from MZL or hairy cell leukemia variant. As in Jeko1, we observed a reduction in cell viability four days
205 after LNA electroporation (Fig.S4B). However, HAIRM did not exhibit permanent changes in proliferation
206 or drug sensitivity (Fig S4C).

207 We also examined ADARreg expression in a cohort of MCL patients, where higher ADARreg expression
208 correlated with poorer overall survival (Fig.5D). ADARreg expression was negatively correlated with
209 ADAR1 (Fig.5E, top) and positively correlated with ADAR2 (coded by ADARB1) (Fig.5E, bottom).

210 While ADARreg knockdown did not significantly alter ADAR transcription (Fig.S4D), it did shift the isoform
211 ratio of ADARB1 in ibrutinib-resistant VL51 cells. Three ADARB1 isoforms upregulated during resistance
212 were significantly repressed after ADARreg knockdown: ADARB1-214, which skips exon 7, resulting in a
213 slightly longer protein (ADAR2b) with lower enzymatic activity, and two untranslated alternatively spliced
214 transcripts (Fig.5F)[26, 27].

215 Immunoblotting confirmed that ADARreg knockdown did not affect ADAR1 levels (Fig.S4E) or subcellular
216 distribution (Fig.S4F). However, ADAR2 did not change in total level but showed increased nuclear
217 translocation, likely enhancing intronic RNA editing (Fig 5G, S5G). ADARreg was also mainly nuclear, in line
218 with its putative role in regulating intronic editing (Fig.S4H).

219 **ADARreg and lncPCED1b maintain the BCR inactivation by altering RNA homeostasis**

220 Transcriptomic analysis of the ibrutinib-resistant VL51 cells after ADARreg or lncPCED1b knockdown
221 (Table S7) revealed significant enrichment of genesets related to the proteasome, spliceosome, and RNA
222 degradation among the transcripts more expressed in resistant cells compared to parental cells (Fig.6A).
223 Inhibiting these elncRNAs, we also reversed genesets normally suppressed by BTK inhibition, in resistant
224 cells, confirming the reactivation of BCR dependency (Fig.6A). ADARreg and lncPCED1b inhibition reverted
225 the SMZL signature associated with ibrutinib-resistance, confirming their role in maintaining the resistant
226 phenotype (Fig.6A). Furthermore, resistant cells had lower expression of genes involved in interferon
227 response compared to parental cells. Still, ADARreg and lncPCED1b silencing reactivated immune
228 responses through PRR signaling (Fig.6A, Table S8). Specifically, ADARreg knockdown restored the
229 expression of interferon-stimulated genes (ISGs) such as IFIH1 and DHX58, which encode critical proteins
230 in the RIG-I-like receptor (RLR) pathway that induces interferon production after detecting unedited
231 dsRNA, normally suppressed by ADAR editing [26] (Fig.6B).

232 **ADARreg modulates IRF3 activity**

233 Since A-to-I RNA editing can influence transcript stability [28], we assessed post-transcriptional
234 modulation of transcript abundance using exon-intron split analysis (EISA). Cells with ADARreg or
235 lncPCED1b knockdown exhibited increased transcript stability, particularly ADARreg kd cells (106
236 stabilized transcripts compared to 64 for lncPCED1b) (Fig.6C, Fig.S5B, Table S9). This aligned with reducing
237 many enzymes involved in RNA degradation in our models. The stabilized transcripts were involved in
238 metabolism pathways and viral infection response (Fig.6D), while lncPCED1b knockdown primarily
239 stabilized transcripts encoding proteasome components (Fig.S5B). Notably, IRF3, a key transcription factor
240 in immune response, was post-transcriptionally regulated by ADARreg. ADARreg kd stabilized the isoform
241 IRF3-203, encoding for the active IRF3, while destabilized IRF3-202, encoding for the dominant-negative
242 IRF3a, which is retained in the cytoplasm (Fig.6E, S5C) [29]. This shift in isoform balance was confirmed at
243 the protein level (Fig.6F, S5D), and immunofluorescence demonstrated increased nuclear localization of
244 IRF3 after ADARreg knockdown (Fig.6G, S5E). In resistant cells, ADARreg expression reduced all IRF3
245 transcripts, with the active IRF3-203 isoform completely depleted (Fig.6E, S5C). After ADARreg
246 knockdown, IRF3 target genes, typically downregulated in resistant cells, were reactivated (Fig.S5F).

247 **ADARreg alters STING and NF-kB signaling**

248 The cGAS-STING pathway is a major regulator of IRF3 [30]. The ibrutinib-resistant VL51 cells upregulated
249 STING but favored an alternative translation initiation (Fig.7A), producing a dominant-negative STINGβ
250 (encoded by STING1-216), which disrupts STING signaling [31]. ADARreg knockdown reverted the ratio
251 between STING and STINGβ, restoring proper signaling (Fig.7A). Indeed, the STING agonist diABZI (10 µM)
252 enhanced BTK inhibition in resistant cells like ADARreg knockdown, which further increased the synergism
253 between ibrutinib and STING agonist in ibrutinib-resistant cells (Fig.7B). A similar mechanism propagated
254 further downstream, with STING triggering NF-κB [30]. In resistant cells, ADARreg altered RELA
255 transcription, producing an inactive N-terminal fragment of p65 (Fig.7C). ADARreg knockdown restored
256 the balance between active p65 and its inhibitory N-terminal fragment at both the RNA (Fig.7C) and
257 protein level (Fig.7D, S6A). This event was translated into higher nuclear translocation of NF-κB after
258 ADARreg knockdown (Fig.7E). However, lncPCED1b knockdown only increased active p65 without
259 affecting the inhibitory form, which explains its lesser nuclear NF-κB compared to ADARreg knockdown.
260 (Fig.7D). Similarly, the phosphorylation of full-length p65 after BCR stimulation increased in resistant cells
261 after ADARreg but not after lncPCED1b knockdown (Fig.S6B).

262 **ADARreg alters transcript usage across key genes**

263 We detected alternative transcripts in key genes as ADARB1 (Fig.5F), IRF3 (Fig.6E), STING (Fig.7A) and RELA
264 (Fig.7C), so we investigated whether ADARreg knockdown generally affected transcript usage.
265 Transcriptome analysis showed that ADARreg knockdown induced widespread alternative transcript
266 usage, affecting 1,536 genes, while lncPCED1b knockdown altered only 469 genes (Fig.7F, 7S6C, Table
267 S10). Many of these isoform changes were linked to intronic editing, with ADARreg affecting 160 genes
268 and lncPCED1b affecting 63 genes (Fig.7S6C). Nineteen of these genes were common to both and primarily
269 involved in p53 regulation after DNA damage (Fig.S6 D, E). Variations in 3'UTR editing were rarely
270 associated with isoform changes (Fig 7F). Some genes with sequence-specific editing, ENO1, RPS3,
271 CLEC2D, MFN1, and AUTS2, showed alternative transcript usage after ADARreg knockdown, with RPS3
272 being similarly affected by lncPCED1b knockdown (Fig.7F, 7S6C). Ribosomal protein S3 (*rpS3*), a
273 multifunctional protein involved in translation, DNA repair, apoptosis, and immune regulation, interacts
274 with p65 to activate specific genes [33]. The expression of the N-terminal fragment of p65 inhibits the
275 RPS3-specific signature [28]. RPS3 has different domains responsible for apoptosis and DNA damage
276 (Fig.7G)[34]. ADARreg and lncPCED1b knockdown restored expression of the RPS3-208 isoform, which
277 was absent in resistant cells (Fig.7H). This isoform lacks the DNA repair domain but retains the apoptosis-
278 inducing and p65-interacting domains (Fig.7G).

279 **ADARreg inhibits NK cell-mediated cytotoxicity**

280 ADARreg knockdown modulated the isoforms of LLT1 (encoded by *CLEC2D* gene), a ligand for the CD161
281 (NKR-P1A) receptor expressed on NK and T cells [35, 36] (Fig.7I). Along with the modulation of IRF3, this
282 suggested that ADARreg knockdown could increase NK cell-mediated killing of resistant cells. Co-culturing
283 ADARreg knockdown VL51 cells with NK cells from a healthy donor resulted in significantly higher NK cell-
284 mediated killing than control cells (Fig.8A, S7A). Additionally, NK cells survived longer in co-cultures with
285 ADARreg knockdown cells (Fig.S7B).

286 To validate these findings, we used publicly available single-cell RNA seq of four chronic lymphocytic
287 leukemia (CLL) patients undergoing ibrutinib treatment [37]to validate these findings. Using genes altered
288 by stable ADARreg kd as a surrogate for ADARreg level (undetectable in polyA datasets), we compared
289 CLL cells from two fast and two slow responders (Fig.S7C). Transcriptomic profiles of surviving cells after
290 treatment resembled the SMZL ADARreg^{high}-resistant model (Fig.S7C). Similar cells were also more
291 abundant at pretreatment time point in slow responders (Fig.S7C). We analyzed NK cells in untreated
292 samples, annotating them as cytotoxic, inflammatory, or tumor-associated NK (TANK) cells (Fig.S7D) [38],
293 and analyzed cell-cell communication using CellChat (Fig.8B, S8). At pretreatment, in a slow responder,
294 ADARreg^{high}-like B cells increased CLEC2D-CD161 interactions with active NKs, compared to ADARreg^{low}-
295 like B cells (Fig.8B). Conversely, ADARreg^{low}-like B cells interacted more with TANK cells through CD99-
296 PILRA signaling, recently associated with favorable immunotherapy outcomes [39] (Fig.8B). No differences
297 in cell communication between ADARreg $^{high/low}$-like B and NK cells were significant in the fast responder
298 (Fig. S8). Tumor cells persisting after treatment had higher CLEC2D expression and ADARreg signature in
299 both patients (Fig.8C). However, those cells were more abundant in slow than fast responder (Fig.8C). In
300 summary, ADARreg modulated CLEC2D isoform balance, favoring NK inhibition in IBR-resistant cells in
301 vitro. A transcriptional program like the one controlled by ADARreg linked high CLEC2D expression to
302 ibrutinib-resistance in CLL patients.

303

304 **Discussion**

305 This study demonstrated that LOC730338, which we renamed ADARreg, can affect the sensitivity to the
306 BTK inhibitor ibrutinib and play a key role in maintaining immune suppression in lymphoma cells. We
307 linked ADARreg to the regulation of the inflammatory response at multiple levels. ADARreg repressed IRF3
308 transcriptionally and post-transcriptionally. It reduced A-to-I editing of intronic regions, affecting the
309 alternative splicing of genes that stimulate an innate immune response. Without ADARreg, the BCR
310 signaling was reactivated, making the B cells more likely to be killed by NK cells.

311 In the presence of pathogens, PRRs activate pathways such as NF-κB, MAPK, and type-I interferon [40,
312 41]. This response must be tightly regulated to prevent overactivation without a real need [35]. ADAR1
313 and ADAR2, through A-to-I RNA editing, play a central role in preventing excessive immune activation by
314 editing self-dsRNA [42]. They also restrain the inflammatory response, modulating the stability and
315 alternative splicing of transcripts mainly involved in antiviral response[43]. Indeed, A-to-I editing can
316 drastically alter RNA's structural and coding properties [44]**.** In detail, A-to-I editing by ADAR2 can convert
317 an intronic AA dinucleotide into an AI dinucleotide that can act like the canonical AG 3' splice site acceptor,
318 impacting splicing events [45]. Our findings add a new layer of complexity to this regulatory network, as
319 we observed significant alterations in these mechanisms following ADARreg knockdown. Splicing was
320 strongly impaired by ADARreg knockdown that reduced the expression of many genes, such as DHX8,
321 DDX42, SF3B1, or PUS7.

322 Although ADARreg was previously associated with RNA editing, its exact role remained unclear [19]. We
323 showed that silencing ADARreg disrupts RNA editing, not by directly regulating ADAR expression, but by
324 possibly changing the intracellular distribution and target interactions of ADARs, particularly ADAR2. The
325 latter, a less abundant but more sequence-specific editor than ADAR1, was most affected by ADARreg

326 knockdown. This led to impaired editing, especially outside repetitive Alu sequences, in line with an
327 ADAR2-dependent mechanism [26, 27]. We hypothesize that ADARreg limits ADAR2's ability to edit
328 introns, influencing alternative transcript usage.

329 Alternative splicing is a critical regulatory mechanism in genes involved in innate immunity, such as cGAS,
330 STING, TBK, and IRF3 [31, 47, 48]. We observed that ADARreg knockdown altered the splicing of STING
331 and IRF3, which are key components of immune signaling. More broadly, ADARreg impacted the
332 alternative splicing of many genes involved in DNA damage repair, supporting its broader role in
333 maintaining RNA homeostasis in resistant cells.

334 ADAR2 has previously been proposed as a potential tumor suppressor in glioma [49] , and cancer often
335 takes advantage of alternative splicing to promote the expression of pro-tumorigenic isoforms [45, 50].
336 Furthermore, tumor cells, which often release fragmented DNA, can evade immune detection by
337 dampening DNA damage-associated molecular patterns (DAMPs), decreasing antitumoral immune
338 attacks. ADARreg may contribute to this immune evasion mechanism by modulating alternative splicing
339 and inhibiting interferon responses.

340 In addition to the alternative transcript usage of IRF3 and STING, ADARreg affected immune signaling by
341 regulating the NF-κB signaling. We observed the production of an alternative form of p65, which retains
342 the ribosomal protein RPS3 in the cytoplasm. RPS3, beyond its ribosomal functions, is involved in
343 apoptosis, DNA repair, and transcriptional regulation [51]. RPS3 was identified as a non-Rel subunit of NF-
344 κB [33] and has already been reported to be involved in cell proliferation and drug resistance in multiple
345 myeloma [52]. RPS3 was our model's most heavily edited and alternatively spliced gene under ADARreg
346 control. The precise role of RPS3 in SMZL growth and BCR pathway activation remains to be elucidated.

347 Our findings suggest that ADARreg works within a broader epigenetic network of ncRNAs that regulate
348 intronic editing and alternative transcript usage. lncPCED1b knockdown showed similar effects, mirroring
349 ADARreg's influence on transcriptomic alterations. ADARreg also regulates the editing of relevant ncRNAs,
350 including lncPCED1b. It is possible that lncPCED1b, like others, might be a mediator of ADARreg action.
351 This is consistent with recent findings linking elncRNA splicing to enhancer activity[41]. We propose that
352 ADARreg, modulating ADAR2 accessibility to subsets of elncRNAs, depending on the presence of a
353 consensus sequence, can regulate their processing and, in turn, the balance of protumoral transcriptional
354 isoforms.

355 ADARreg silencing reactivates the INF-I response and modulates surface receptors such as LLT1, increasing
356 SMZL cells' immunogenicity and susceptibility to NK cell-mediated cytotoxicity. In SMZL patients, poorer
357 outcomes are associated with an immune-suppressive phenotype with immune checkpoint activation
358 [53]. These patients often exhibit KLF2 and NOTCH2 mutations, but a clear mechanism for immune escape
359 is missing. ADARreg may be a critical factor influencing tumor-microenvironment interactions.

360 This mechanism was further validated in CLL patients, where we observed a link between the selection of
361 tumor clones resistant to BCR inhibition and the suppression of an immunological signature modulated
362 by ADARreg. Moreover, an ADARreg^{high}-signature in hematological tumors, such as MZL, CLL, and MCL,
363 may indicate an unfavorable prognosis for patients treated with BCR signaling inhibitors. Conversely,
364 ADARreg represents a promising therapeutic target for antisense oligonucleotide strategies to elicit
365 spontaneous immune responses against immune-suppressive cells.

Funding

This work was partially supported by the Swiss National Science Foundation grants CRSK-3_190808, SNSF 310030_197466, and SNSF 31003A_163232/1). NM was supported by a Ph.D. Fellowship of the NCCR RNA & Disease, a National Center of Competence in Research funded by the Swiss National Science Foundation (grant numbers 182880 and 205601). SR was funded by Science Foundation Ireland under Grant number [18/CRT/6214] and in part by the EU's Horizon 2020 research and innovation program under the Marie Sklodowska-Curie grant H2020-MSCA-COFUND-2019-945385.

Disclosure of Potential Conflicts of Interest

Luciano Cascione: institutional research funds from Orion; travel grant from HTG. Alberto J. Arribas: travel grant from Astra Zeneca, consultant for PentixaPharm. Chiara Tarantelli: travel grant from iOnctura. Francesco Bertoni: institutional research funds from ADC Therapeutics, Bayer AG, BeiGene, Floratek Pharma, Helsinn, HTG Molecular Diagnostics, Ideogen AG, Idorsia Pharmaceuticals Ltd., Immagene, ImmunoGen, Menarini Ricerche, Nordic Nanovector ASA, Oncternal Therapeutics, Spexis AG; consultancy fee from BIMINI Biotech, Helsinn, Menarini; advisory board fees to institution from Novartis; expert statements provided to HTG Molecular Diagnostics; travel grants from Amgen, Astra Zeneca, Beigene, InnoCare, iOnctura. The other Authors have nothing to disclose.

References

1. Rossi, D., F. Bertoni, and E. Zucca, *Marginal-Zone Lymphomas.* N Engl J Med, 2022. **386**(6): p. 568-581.
2. Petro, J.B., et al., *Bruton's tyrosine kinase is required for activation of IkappaB kinase and nuclear factor kappaB in response to B cell receptor engagement.* J Exp Med, 2000. **191**(10): p. 1745-54.
3. Stanchina, M.D., et al., *Navigating the changing landscape of BTK-targeted therapies for B cell lymphomas and chronic lymphocytic leukaemia.* Nat Rev Clin Oncol, 2024. **21**(12): p. 867-887.
4. Noy, A., et al., *Targeting Bruton tyrosine kinase with ibrutinib in relapsed/refractory marginal zone lymphoma.* Blood, 2017. **129**(16): p. 2224-2232.
5. Opat, S., et al., *The MAGNOLIA Trial: Zanubrutinib, a Next-Generation Bruton Tyrosine Kinase Inhibitor, Demonstrates Safety and Efficacy in Relapsed/Refractory Marginal Zone Lymphoma.* Clin Cancer Res, 2021. **27**(23): p. 6323-6332.
6. Deng, L., et al., *Orelabrutinib for the treatment of relapsed or refractory marginal zone lymphoma: A phase 2, multicenter, open-label study.* Am J Hematol, 2023. **98**(11): p. 1742-1750.
7. Stephens, D.M. and J.C. Byrd, *Resistance to Bruton tyrosine kinase inhibitors: the Achilles heel of their success story in lymphoid malignancies.* Blood, 2021. **138**(13): p. 1099-1109.
8. Wang, H., et al., *The resistance mechanisms and treatment strategies of BTK inhibitors in B-cell lymphoma.* Hematol Oncol, 2021. **39**(5): p. 605-615.
9. Shaffer, A.L., 3rd, et al., *Overcoming Acquired Epigenetic Resistance to BTK Inhibitors.* Blood Cancer Discov, 2021. **2**(6): p. 630-647.
10. Zhao, X., et al., *Transcriptional programming drives Ibrutinib-resistance evolution in mantle cell lymphoma.* Cell Rep, 2021. **34**(11): p. 108870.
11. Arribas, A.J., et al., *Resistance to PI3Kdelta inhibitors in marginal zone lymphoma can be reverted by targeting the IL-6/PDGFRA axis.* Haematologica, 2022. **107**(11): p. 2685-2697.

408 12. Arribas, A.J., et al., *ERBB4-Mediated Signaling Is a Mediator of Resistance to PI3K and BTK*
409 *Inhibitors in B-cell Lymphoid Neoplasms.* Mol Cancer Ther, 2024. **23**(3): p. 368-380.
410 13. Mattick, J.S., et al., *Long non-coding RNAs: definitions, functions, challenges and*
411 *recommendations.* Nat Rev Mol Cell Biol, 2023. **24**(6): p. 430-447.
412 14. Andersson, R., et al., *An atlas of active enhancers across human cell types and tissues.* Nature,
413 2014. **507**(7493): p. 455-461.
414 15. Lai, F., et al., *Activating RNAs associate with Mediator to enhance chromatin architecture and*
415 *transcription.* Nature, 2013. **494**(7438): p. 497-501.
416 16. Saha, D., et al., *Enhancer switching in cell lineage priming is linked to eRNA, Brg1's AT-hook, and*
417 *SWI/SNF recruitment.* Mol Cell, 2024. **84**(10): p. 1855-1869 e5.
418 17. Agirre, X., et al., *Long non-coding RNAs discriminate the stages and gene regulatory states of*
419 *human humoral immune response.* Nat Commun, 2019. **10**(1): p. 821.
420 18. Napoli, S., et al., *Characterization of GECPAR, a noncoding RNA that regulates the transcriptional*
421 *program of diffuse large B-cell lymphoma.* Haematologica, 2022. **107**(5): p. 1131-1143.
422 19. Giacopuzzi, E., et al., *Genome-wide analysis of consistently RNA edited sites in human blood*
423 *reveals interactions with mRNA processing genes and suggests correlations with cell types and*
424 *biological variables.* BMC Genomics, 2018. **19**(1): p. 963.
425 20. Inokuchi, K., et al., *Establishment and characterization of a villous lymphoma cell line from splenic*
426 *B-cell lymphoma.* Leuk Res, 1995. **19**(11): p. 817-22.
427 21. Arribas, A., et al., *IL16 PRODUCTION IS A MECHANISM OF RESISTANCE TO BTK INHIBITORS AND*
428 *TO R-CHOP.* Hematological Oncology, 2023. **41**(S2): p. 188-189.
429 22. Jha, S. and J. Pan-Yun Ting, *Holding the inflammatory system in check: NLRs keep it cool.*
430 F1000Prime Rep, 2015. **7**: p. 15.
431 23. Whyte, W.A., et al., *Master transcription factors and mediator establish super-enhancers at key*
432 *cell identity genes.* Cell, 2013. **153**(2): p. 307-19.
433 24. Consortium, F., et al., *A promoter-level mammalian expression atlas.* Nature, 2014. **507**(7493): p.
434 462-70.
435 25. Alerasool, N., et al., *An efficient KRAB domain for CRISPRi applications in human cells.* Nat
436 Methods, 2020. **17**(11): p. 1093-1096.
437 26. Sinigaglia, K., et al., *ADAR RNA editing in innate immune response phasing, in circadian clocks and*
438 *in sleep.* Biochim Biophys Acta Gene Regul Mech, 2019. **1862**(3): p. 356-369.
439 27. Hajji, K., et al., *ADAR2 enzymes: efficient site-specific RNA editors with gene therapy aspirations.*
440 RNA, 2022. **28**(10): p. 1281-1297.
441 28. Brummer, A., et al., *Structure-mediated modulation of mRNA abundance by A-to-I editing.* Nat
442 Commun, 2017. **8**(1): p. 1255.
443 29. Li, C., L. Ma, and X. Chen, *Interferon regulatory factor 3-CL, an isoform of IRF3, antagonizes activity*
444 *of IRF3.* Cell Mol Immunol, 2011. **8**(1): p. 67-74.
445 30. Yum, S., et al., *TBK1 recruitment to STING activates both IRF3 and NF-kappaB that mediate*
446 *immune defense against tumors and viral infections.* Proc Natl Acad Sci U S A, 2021. **118**(14).
447 31. Liang, J., et al., *The Alternatively Spliced Isoforms of Key Molecules in the cGAS-STING Signaling*
448 *Pathway.* Front Immunol, 2021. **12**: p. 771744.
449 32. Gao, X. and P.R. Hardwidge, *Ribosomal protein s3: a multifunctional target of attaching/effacing*
450 *bacterial pathogens.* Front Microbiol, 2011. **2**: p. 137.
451 33. Wan, F., et al., *Ribosomal protein S3: a KH domain subunit in NF-kappaB complexes that mediates*
452 *selective gene regulation.* Cell, 2007. **131**(5): p. 927-39.
453 34. Jang, C.Y., J.Y. Lee, and J. Kim, *RpS3, a DNA repair endonuclease and ribosomal protein, is involved*
454 *in apoptosis.* FEBS Lett, 2004. **560**(1-3): p. 81-5.

455 35. Braud, V.M., et al., *LLT1-CD161 Interaction in Cancer: Promises and Challenges.* Front Immunol,
456 2022. **13**: p. 847576.
457 36. Germain, C., et al., *Characterization of alternatively spliced transcript variants of CLEC2D gene.* J
458 Biol Chem, 2010. **285**(46): p. 36207-15.
459 37. Rendeiro, A.F., et al., *Chromatin mapping and single-cell immune profiling define the temporal*
460 *dynamics of ibrutinib response in CLL.* Nat Commun, 2020. **11**(1): p. 577.
461 38. Tang, F., et al., *A pan-cancer single-cell panorama of human natural killer cells.* Cell, 2023. **186**(19):
462 p. 4235-4251 e20.
463 39. Li, Q., et al., *Comprehensive analysis of PILRAlpha's association with the prognosis, tumor immune*
464 *infiltration, and immunotherapy in pan-cancer.* Sci Rep, 2023. **13**(1): p. 14334.
465 40. Lanng, K.R.B., E.L. Lauridsen, and M.R. Jakobsen, *The balance of STING signaling orchestrates*
466 *immunity in cancer.* Nat Immunol, 2024. **25**(7): p. 1144-1157.
467 41. Tan, J.Y. and A.C. Marques, *The activity of human enhancers is modulated by the splicing of their*
468 *associated lncRNAs.* PLoS Comput Biol, 2022. **18**(1): p. e1009722.
469 42. Li, Q., et al., *RNA editing underlies genetic risk of common inflammatory diseases.* Nature, 2022.
470 **608**(7923): p. 569-577.
471 43. Wang, I.X., et al., *ADAR regulates RNA editing, transcript stability, and gene expression.* Cell Rep,
472 2013. **5**(3): p. 849-60.
473 44. Shevchenko, G. and K.V. Morris, *All I's on the RADAR: role of ADAR in gene regulation.* FEBS Lett,
474 2018. **592**(17): p. 2860-2873.
475 45. Tang, S.J., et al., *Cis- and trans-regulations of pre-mRNA splicing by RNA editing enzymes influence*
476 *cancer development.* Nat Commun, 2020. **11**(1): p. 799.
477 46. Martinez, N.M., et al., *Pseudouridine synthases modify human pre-mRNA co-transcriptionally and*
478 *affect pre-mRNA processing.* Mol Cell, 2022. **82**(3): p. 645-659 e9.
479 47. Li, Y., et al., *Identification of novel alternative splicing variants of interferon regulatory factor 3.*
480 Biochim Biophys Acta, 2011. **1809**(3): p. 166-75.
481 48. Lee, F.F.Y. and S. Alper, *Alternative pre-mRNA splicing as a mechanism for terminating Toll-like*
482 *Receptor signaling.* Front Immunol, 2022. **13**: p. 1023567.
483 49. Li, Z., et al., *Aberrant alternative splicing pattern of ADAR2 downregulates adenosine-to-inosine*
484 *editing in glioma.* Oncol Rep, 2015. **33**(6): p. 2845-52.
485 50. Sciarrillo, R., et al., *The role of alternative splicing in cancer: From oncogenesis to drug resistance.*
486 Drug Resist Updat, 2020. **53**: p. 100728.
487 51. Wier, E.M., et al., *Identification of an N-terminal truncation of the NF-kappaB p65 subunit that*
488 *specifically modulates ribosomal protein S3-dependent NF-kappaB gene expression.* J Biol Chem,
489 2012. **287**(51): p. 43019-29.
490 52. Chen, G., et al., *Ribosomal protein S3 mediates drug resistance of proteasome inhibitor: potential*
491 *therapeutic application in multiple myeloma.* Haematologica, 2024. **109**(4): p. 1206-1219.
492 53. Bonfiglio, F., et al., *Genetic and phenotypic attributes of splenic marginal zone lymphoma.* Blood,
493 2022. **139**(5): p. 732-747.

494

495 **Main Figures**

496

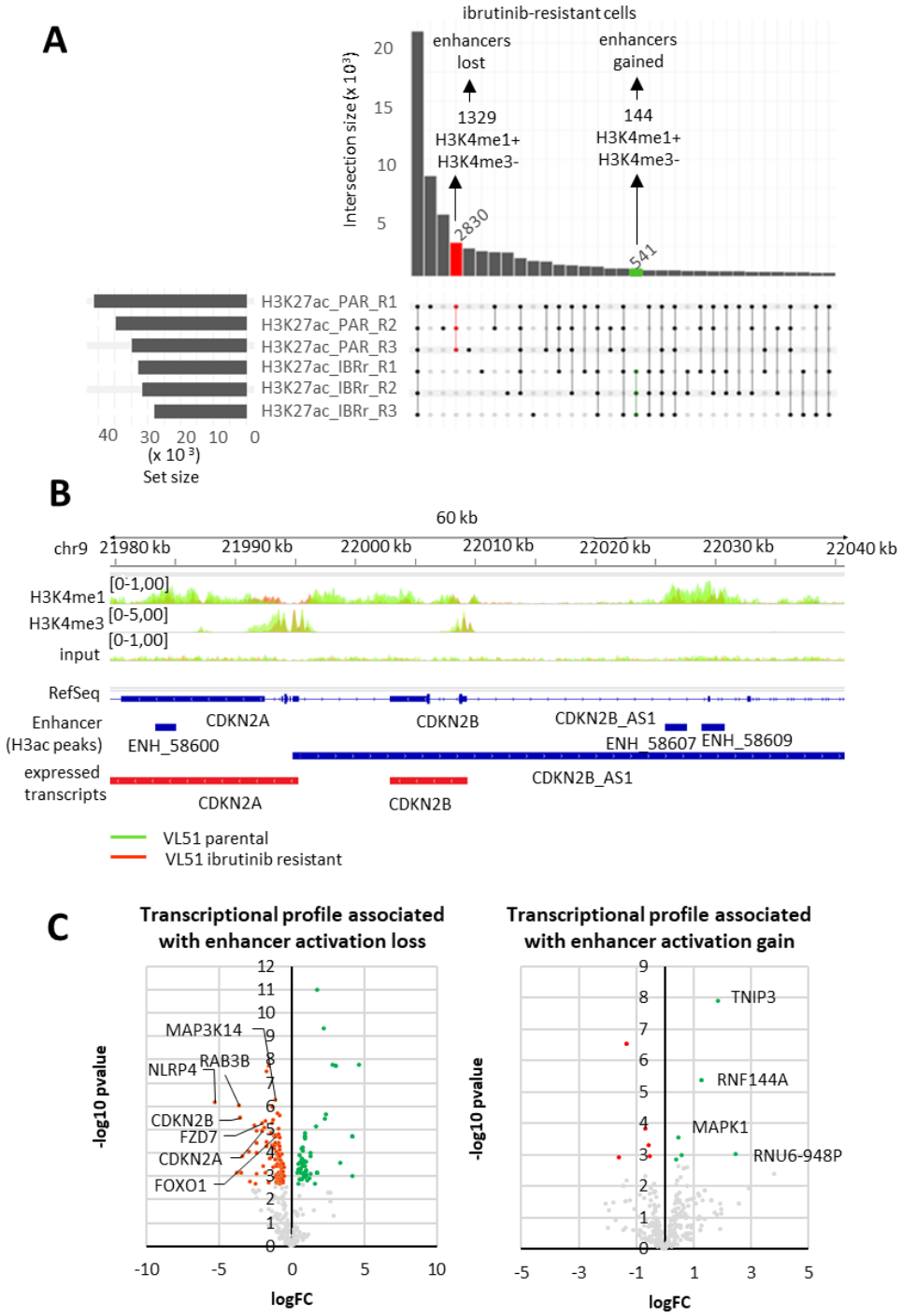

497 **Figure 1. Ibrutinib-resistance is associated with changes in super-enhancer activation**

498

499 **(A)** ChIP-seq H3k27 acetylated peak counts in three independent biological replicates of parental
500 VL51 and ibrutinib-resistant (IBRr) derivatives. The horizontal bars show the number of total
501 peaks in each sample. The red and green bars highlight the number of robust peaks differentially
502 enriched in parental and ibrutinib-resistant cells. The number of *bona fide* enhancers is also
503 indicated based on the co-occurrence of H3K4me1 peak and the absence of H3K4me3.
504 **(B)** Schematic representation of an example of enhancer lost in ibrutinib-resistant cells, close to
505 CDKN2A and CDKN2B loci. H3K4me1, H3K4me3, and input tracks are overlays of parental (green)
506 and ibrutinib-resistant derivatives (red) replicates. Genomic positions of acetylated H3 peaks and
507 transcripts differentially expressed (red blocks) in ibrutinib-resistant versus parental cells are
508 indicated.
509 **(C)** Volcano plot representing the expression of genes mapping within 40kb from an enhancer lost
510 (left) or gained (right) in ibrutinib-resistant cells. Orange dots represent genes significantly
511 downregulated, and green dots represent genes upregulated. The gene symbol of selected
512 interesting genes is displayed.

513

514

515

516

517

518

519

520

521

522

523

524

525

526

527

528

529

530

531

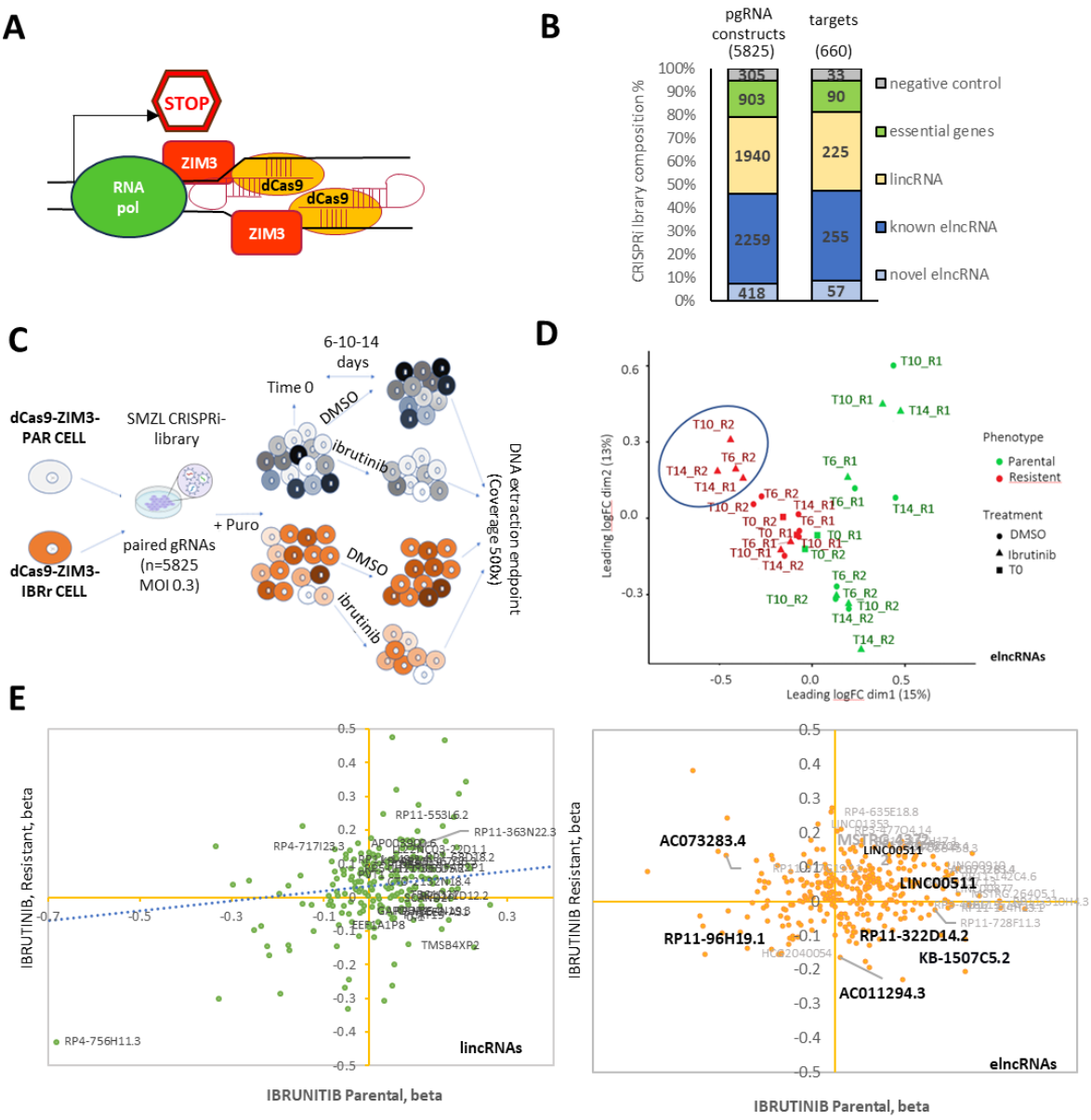

Figure 2. Functional screening of elncRNAs linked to BCR blockade

(A) CRISPRi schematic representation.

(B) Composition of CRISPRi lentiviral library, in terms of the constructs targeting different subtypes of controls and target genes.

(C) Schematic overview of the CRISPRi screen experimental plan.

(D) MDS plots showing the distribution of samples at the beginning of CRISPRi screen (T0, squared labels) or after 6 (T6), 10 (T10) or 14 (T14) days, based on the drop out of elncRNAs. Parental cells are represented in green, ibrutinib-resistant in red. Samples exposed to the drug are labelled with triangle, to the vehicle with the circle. The blue circle highlights the clustering of resistant cells, exposed to ibrutinib.

(E) Scatter plot of β values measuring the drop out of single lincRNAs, left, or elncRNAs, right, in parental cells exposed to ibrutinib for 14 days respect to ibrutinib resistant cells. If the measurement is statistically significant (FDR<0.2) the label with gene symbol is displayed. The bold black label indicates elncRNAs selected for further validation steps.

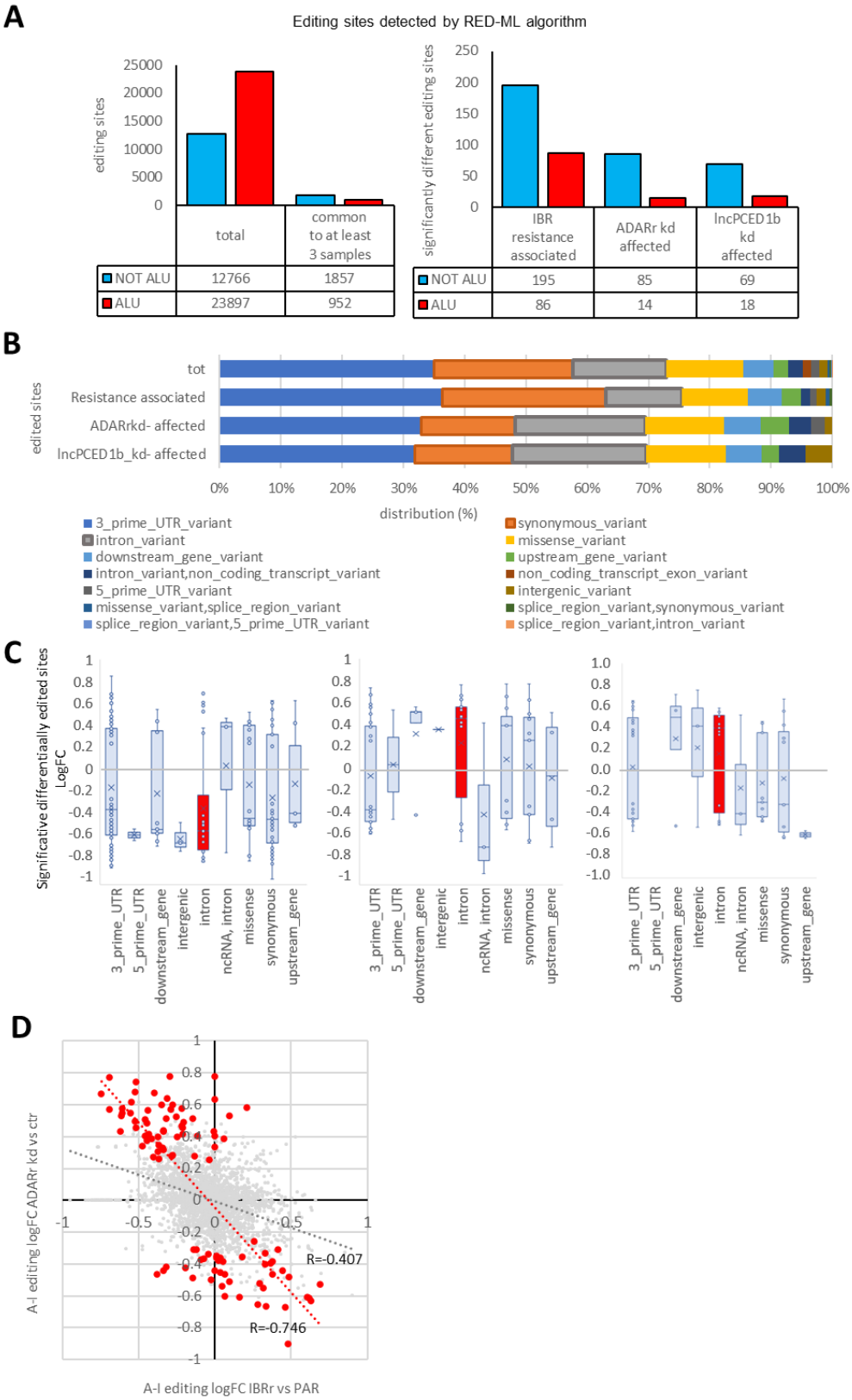

585

586 **Figure 3. ADARreg silencing affects A to I editing in intronic regions.**

587 **(A)** Left, numbers of significative editing sites detected by RED-ML algorithm (FDR< 0.05). Red bars
588 represent the number of editing sites falling within Alu sequences, light blue bars the ones
589 outside. Right, numbers of significative editing sites differentially present in the ibrutinib-
590 resistant cells compared to parental cells, or in ibrutinib resistant ADARreg kd or lncPCED1b kd,
591 respect to the KLK12kd negative control (pvalue< 0.05, Limma test).
592 **(B)** Cumulative bar graphs showing the percentual genomic distribution of the total significative
593 editing sites, or of the significative differentially edited sites in the comparisons of ibrutinib
594 resistant cells versus parental cells, or ibrutinib resistant ADARreg kd or lncPCED1b kd, respect to
595 the KLK12kd negative control cells (pvalue< 0.05, Limma test).
596 **(C)** Log fold change (FC) distribution of differentially not-Alu edited sites within different genomic
597 locations, in the comparison of ibrutinib resistant cells versus parental cells (left), or ibrutinib
598 resistant ADARreg kd (middle) or lncPCED1b kd (right), respect to the KLK12kd negative control
599 cells (pvalue< 0.05, Limma test, mean and outlier values are shown).
600 **(D)** Scatter plots of editing site log FC in the comparison resistant versus parental and ibrutinib
601 resistant ADARreg kd cells versus KLK12kd control. Red dots represent editing sites statistically
602 significant in the comparison ADARreg kd versus control. The regression line represents Pearson
603 correlation (pvalue< 0.05, Limma test).

604

605

606

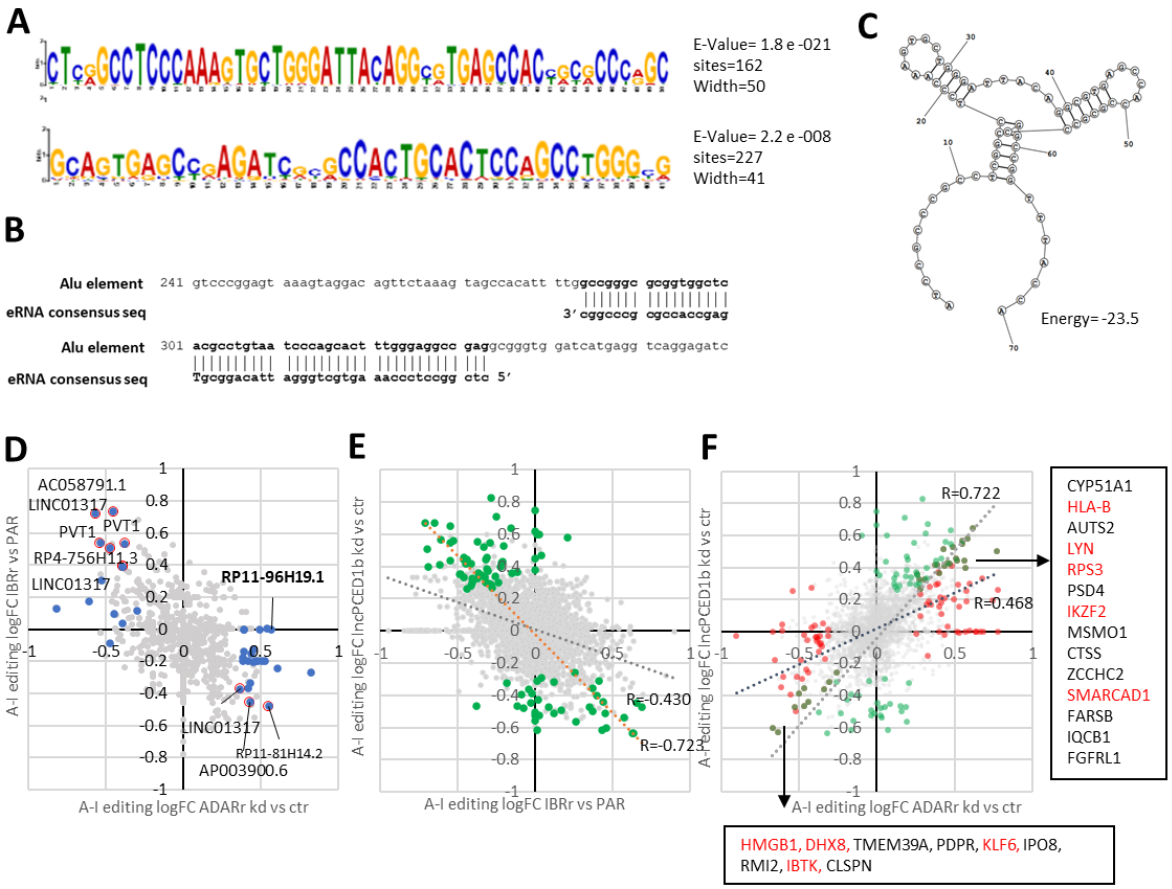

Figure 4. lncPCED1b takes part to editome regulation with ADARreg.

(A) Consensus sequence identified by MEME tool within all SMZL elncRNA sequences (top) or within SMZL super-enhancer DNA sequences.

(B) Alignment of elncRNA consensus sequence and Alu element

(C) RNA structure prediction of the SMZL elncRNA consensus sequence (left) or SMZL super-enhancer DNA consensus sequence (right). Thermodynamic stability of the structure is represented by the energy value calculated by RNAHybrid.

(D) Scatter plots of ncRNA editing site Log FC in the comparison of ibrutinib-resistant ADARreg kd cells versus KLK12 kd control and ibrutinib-resistant versus parental. Blue dots represent significant differentially edited sites after ADARreg knockdown, red circled dots represent those significant differentially edited sites after ADARreg and lncPCED1b knockdown.

(E) Scatter plot of editing site Log FC in the comparison ibrutinib resistant versus parental and ibrutinib resistant lncPCED1b kd cells versus KLK12kd control. Green dots represent editing sites statistically significant in the comparison lncPCED1b kd versus control.

(F) Scatter plot of editing site Log FC in the comparison ibrutinib-resistant ADARreg kd cells versus control and ibrutinib-resistant lncPCED1b kd cells versus control. Red dots represent editing sites statistically significant in the comparison ADARreg kd versus control, green dots in the comparison lncPCED1b kd versus control. Genes that are significantly more or less edited after ADARreg kd and lncPCED1b kd, with respect to the KLK12 kd control, are listed in the boxes. The regression line represents Pearson correlation (pvalue< 0.05, Limma test).

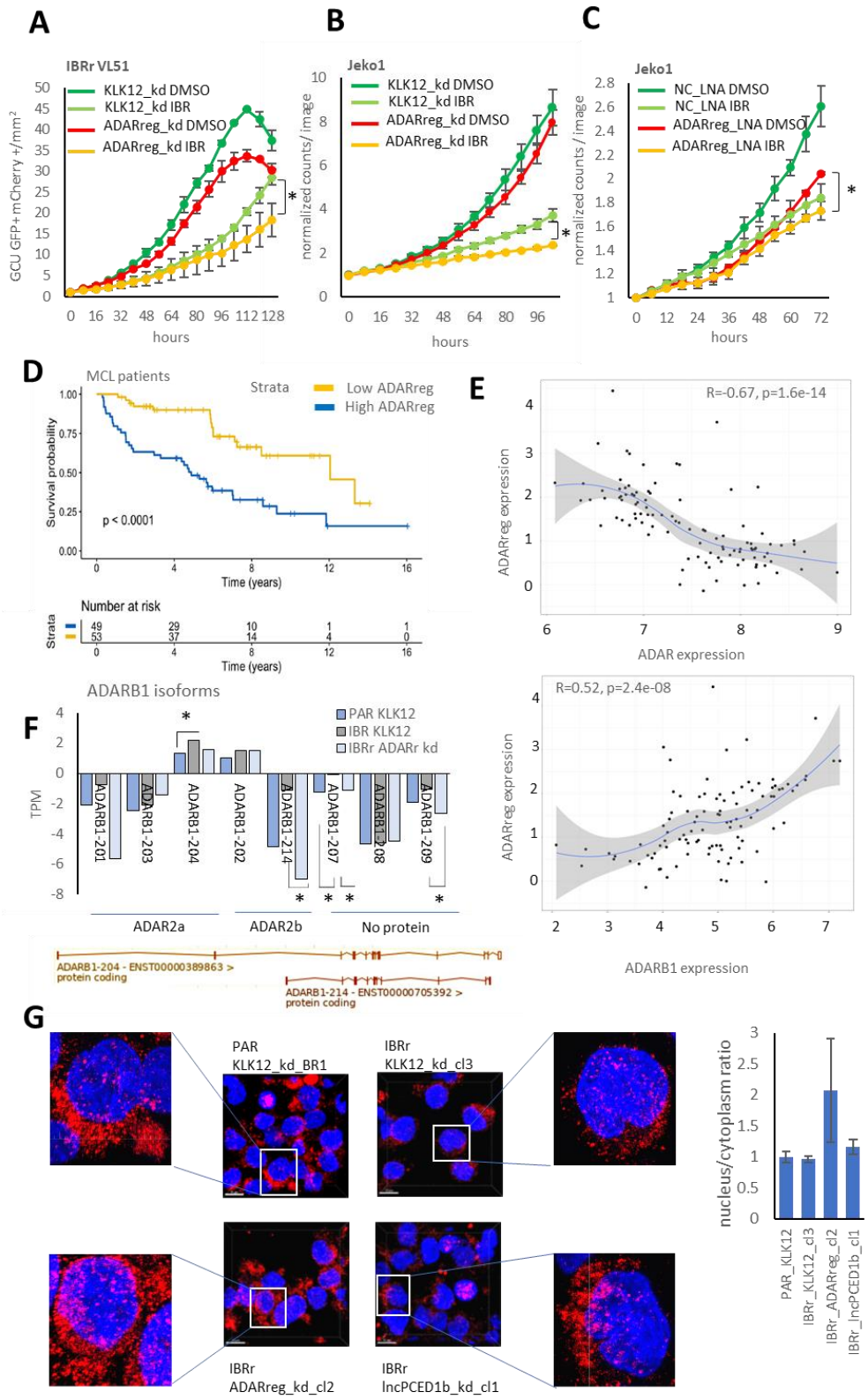

628

629 **Figure 5. ADARreg modulates BTK inhibition response by regulating ADAR2 activity**

630 **(A)** Growth curve of ibrutinib resistant VL51 KLK12 or ADARreg kd built collecting green fluorescence
631 of GFP+ mCherry + cells over 5 days under exposure to ibrutinib or vehicle
632 **(B)** Growth curve of Jeko1 KLK12 or ADARreg kd built counting cells over 4 days under exposure to
633 ibrutinib or vehicle
634 **(C)** Growth curve of Jeko1 seeded 4 days after ADARreg LNA or negative control electroporation and
635 built counting cells over 3 days under exposure to ibrutinib or vehicle.
636 **(D)** The Kaplan-Meyer curve representing the overall survival of n=102 MCL patients dichotomized in
637 n=49 high-level ADARreg expressor and n=53 low-expressor patients.
638 **(E)** Pearson correlation of ADARreg and ADAR, top, or ADARB1, bottom, in 102 MCL patients.
639 **(F)** Top, ADARB1 isoforms measured in total RNAseq performed in parental and ibrutinib resistant
640 VL51 negative control cells and in ibrutinib resistant VL51 ADARreg kd. The corresponding protein
641 isoform is reported at the bottom of the graph. * FDR<0.05. Bottom, schematic representation of
642 the isoforms ADARB1-204 and ADARB1-214.
643 **(G)** Left, immunofluorescence of ADAR2 in parental VL51 or ibrutinib-resistant KLKL12 kd (negative
644 control), top, or ADARreg kd or lncPCED1b kd monoclonal cell lines, bottom. DAPI stained nuclei,
645 blue, Alexa647-conjugated antibody stained ADAR2, red. A blue and red fluorescence overlay was
646 reported; a close-up from each picture shows a single-cell level magnification. Right, graph with
647 nuclei/ cytoplasm ratio of ADAR2 integrated density.

648

649

650

651

652

653

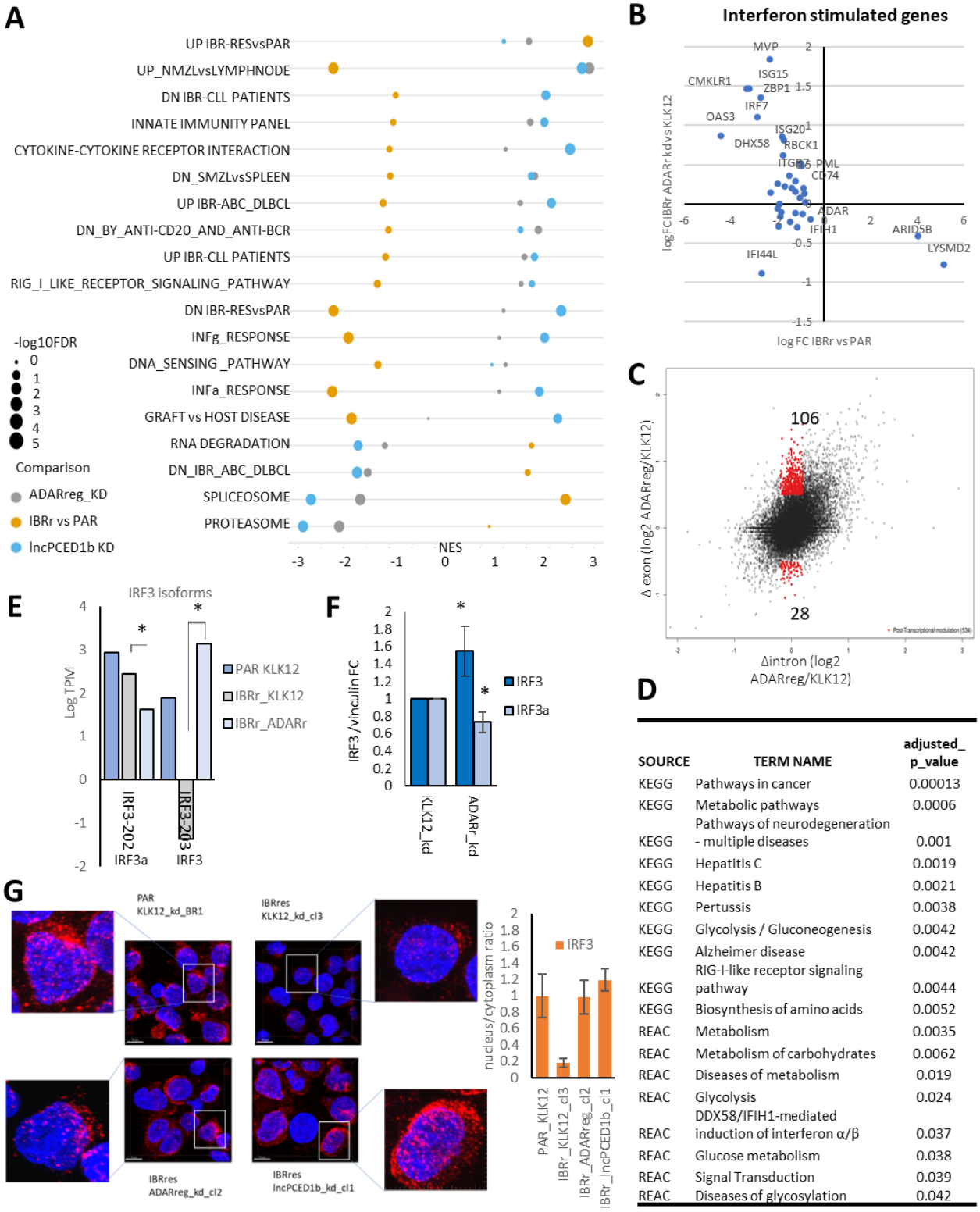

D

SOURCE	TERM NAME	adjusted_ p_value
KEGG	Pathways in cancer	0.00013
KEGG	Metabolic pathways	0.0006
KEGG	Pathways of neurodegeneration - multiple diseases	0.001
KEGG	Hepatitis C	0.0019
KEGG	Hepatitis B	0.0021
KEGG	Pertussis	0.0038
KEGG	Glycolysis / Gluconeogenesis	0.0042
KEGG	Alzheimer disease	0.0042
KEGG	RIG-I-like receptor signaling pathway	0.0044
KEGG	Biosynthesis of amino acids	0.0052
REAC	Metabolism	0.0035
REAC	Metabolism of carbohydrates	0.0062
REAC	Diseases of metabolism	0.019
REAC	Glycolysis	0.024
REAC	DDX58/IFIH1-mediated induction of interferon α/β	0.037
REAC	Glucose metabolism	0.038
REAC	Signal Transduction	0.039
REAC	Diseases of glycosylation	0.042

Figure 6. ADARreg modulates IRF3 activity

(A) Preranked GSEA of RNAseq data in ibrutinib resistant VL51 KLK12 kd respect to parental VL51 KLK12 kd (yellow), after ADARreg knock down in ibrutinib resistant VL51 (grey), or lncPCED1b knock down (blue). Gene sets are represented based on decreasing enrichment score (NES), dot size is representative of statistical significance.

(B) Scatter plot of logFC of interferon-stimulated genes in ibrutinib-resistant cells respect to parental cells and in ibrutinib-resistant cells VL51 ADARreg kd respect to negative control.

(C) Scatter plots representing the comparison of changes in intronic (Δintron) and exonic (Δexon) reads per each expressed transcript in ibrutinib resistant VL51 ADARreg kd respect to KLK12 kd negative control. Δexon/ Δintron=1 reflects transcriptional modulation, Δexon/ Δintron≠1 reflects post-transcriptional modulation. Red dots represent robust post-transcriptionally modulated transcripts. P value<0.05.

(D) gProfiler gene ontology analysis of transcripts significantly modulated at post-transcriptional level after ADARreg kd.

(E) IRF3 isoforms measured in total RNAseq performed in parental and ibrutinib resistant VL51 negative control cells and in ibrutinib resistant VL51 ADARreg kd. The corresponding protein isoform is reported at the bottom of the graph. * FDR<0.05

(F) IRF3 and IRF3a protein level quantification in ibrutinib resistance VL51 negative control cells and ibrutinib resistant VL51 ADARreg kd. Average of two independent biological replicates. * P <0.05

(G) Left, immunofluorescence of IRF3 in parental VL51 or ibrutinib-resistant KLKL12 kd (negative control), top, or ADARreg kd or lncPCED1b kd monoclonal cell lines, bottom. DAPI stained nuclei, blue, Alexa647-conjugated antibody stained IRF3, red. A blue and red fluorescence overlay was reported; a close-up from each picture shows a single-cell level magnification. Right, graph with nuclei/ cytoplasm ratio of IRF3 integrated density.

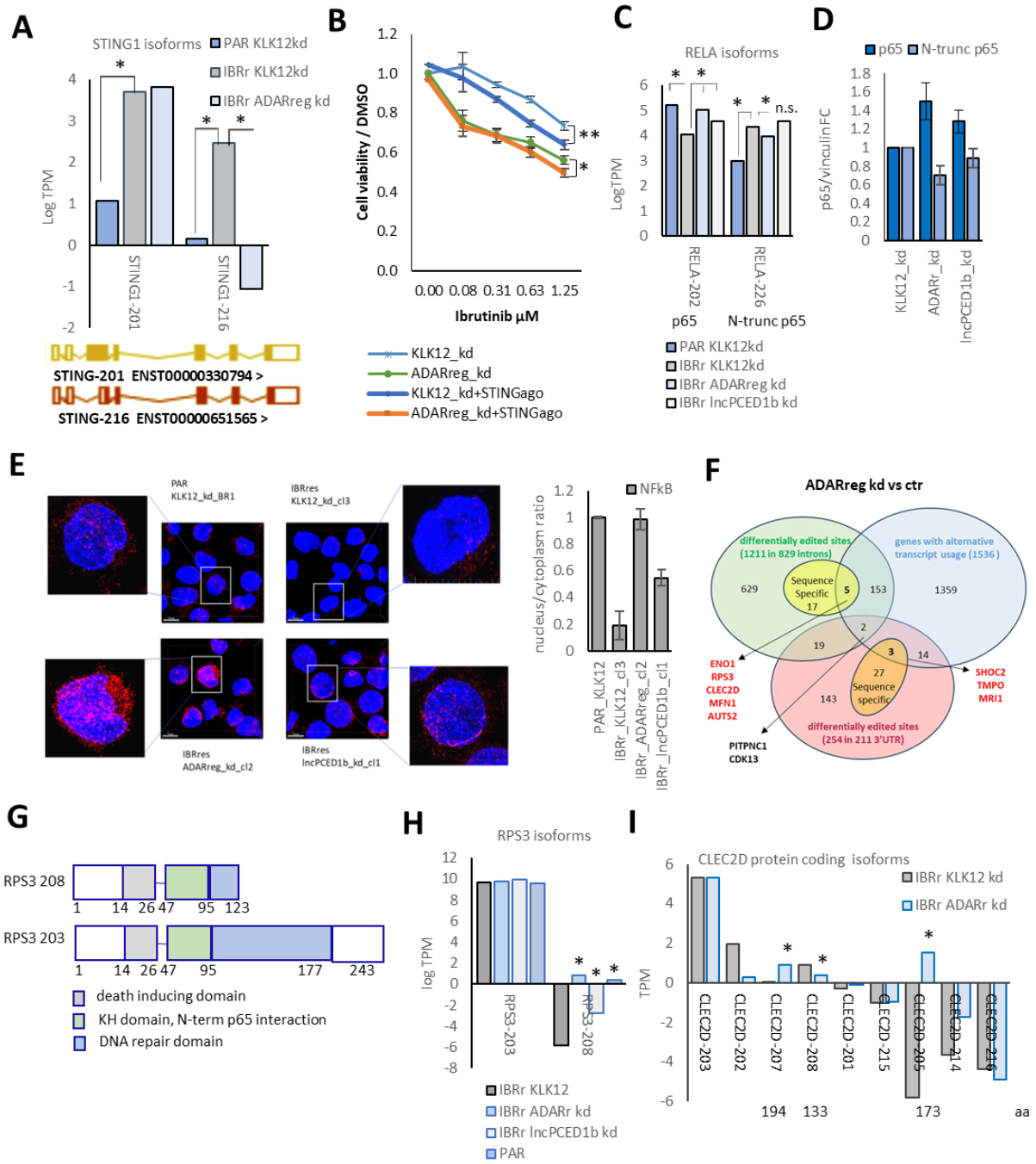

Figure 7. ADARreg alters transcript usage across key genes, like STING and NF-kB.

(A) Top, STING1 isoforms measured in total RNAseq performed in parental and ibrutinib resistant VL51 negative control cells and ibrutinib resistant VL51 ADARreg kd. The corresponding protein isoform is reported at the bottom of the graph. Bottom, schematic representation of the two isoforms, as reported in Ensembl database. White boxes represent untranslated sequences, 5'UTR and 3'UTR. * FDR<0.05

686 **(B)** MTT assay performed in ibrutinib resistant VL51 ADARreg kd or KLK12 kd exposed to increasing
687 doses of ibrutinib alone or in combination with STING agonist diABZI (10 µM), or vehicle for 96 h.
688 Average of three independent biological replicates. * P <0.05.
689 **(C)** Left, RELA isoforms measured in total RNAseq performed in parental and ibrutinib resistant VL51
690 negative control cells and ibrutinib resistant VL51 ADARreg kd. The corresponding protein
691 isoform is reported at the bottom of the graph. * FDR<0.05. Right, Bar graph representing the
692 ratio between the transcript producing the active p65 isoform and the N-terminal truncated p65.
693 **(D)** p65 and N-terminal truncated p65 protein level quantification in ibrutinib-resistant VL51
694 negative control cells and ibrutinib-resistant VL51 ADARreg kd. Average of two independent
695 biological replicates. * P <0.05
696 **(E)** Left, immunofluorescence of NF-kB in parental VL51 or ibrutinib-resistant KLKL12 kd (negative
697 control), top, or ADARreg kd or lncPCED1b kd monoclonal cell lines, bottom. DAPI-stained nuclei,
698 blue, Alexa647-conjugated antibody-stained NF-kB, red. A blue and red fluorescence overlay was
699 reported; a close-up from each picture shows a single-cell level magnification. Right, graph with
700 uclei/ cytoplasm ratio of NF-kB integrated density.
701 **(F)** Venn diagram intersecting total and sequence-specific edited transcripts significantly modulated
702 in introns or 3'UTR and alternative transcriptional isoforms in ibrutinib-resistant VL51 after
703 ADARreg kd.
704 **(G)** Scheme of protein domains in RPS3 isoforms encoded by RPS3-203 or-208 transcripts.
705 **(H)** Left, RPS3 isoforms measured in total RNAseq performed in parental and ibrutinib resistant VL51
706 negative control cells and ibrutinib resistant VL51 ADARreg or lncPCED1b kd. * FDR<0.05. Right,
707 **(I)** CLEC2D isoforms measured in total RNAseq performed in ibrutinib-resistant VL51 negative
708 control cells and ibrutinib-resistant VL51 ADARreg. * FDR<0.05.

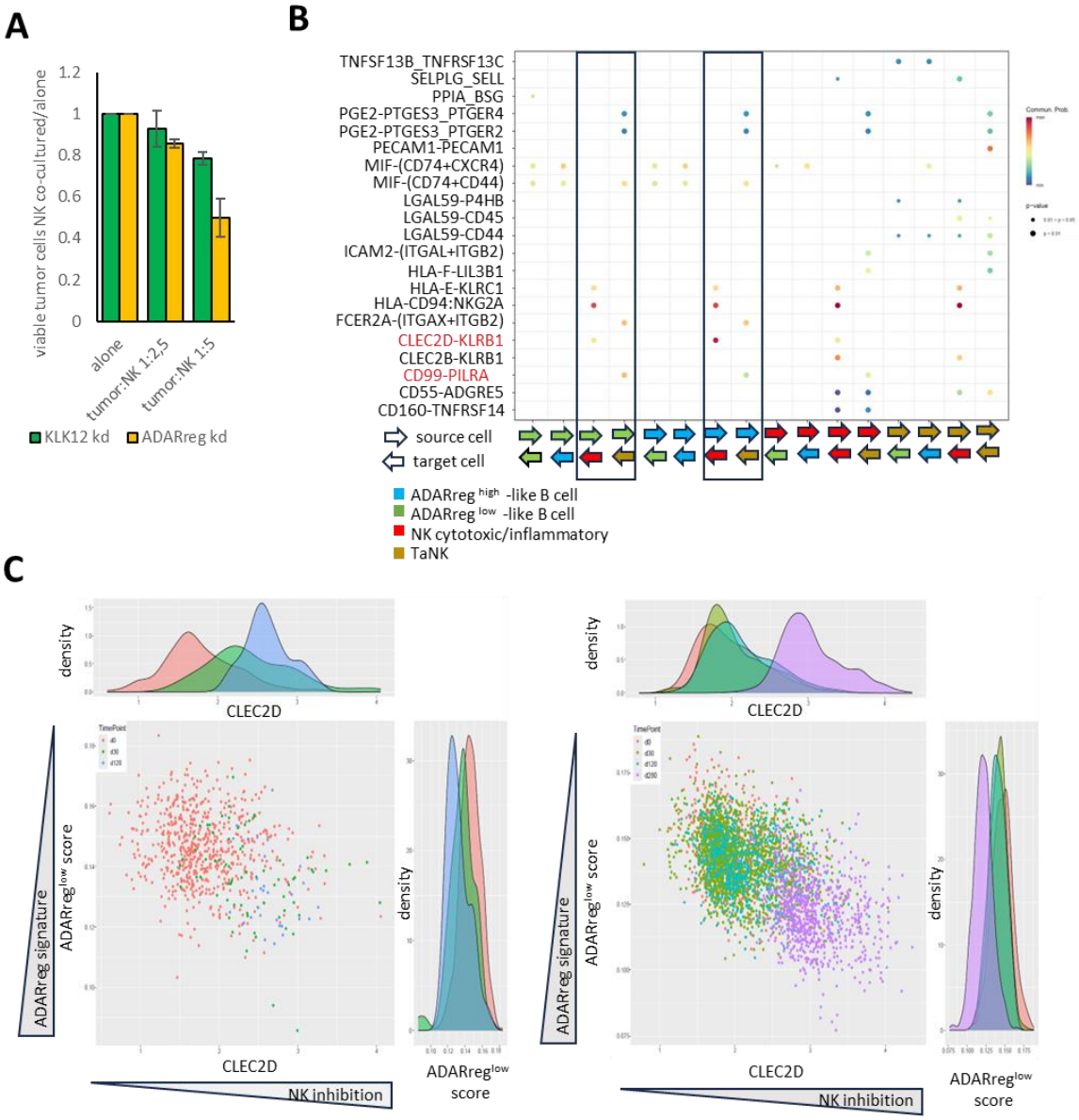

Figure 8. ADARreg inhibits NK cell-mediated cytotoxicity

(A) Bar graph representing viable GFP+ mCherry+ ibrutinib resistant VL51, negative control or ADARreg kd, after 7 days of co-culture with activated healthy donor NK cells, normalized to the number of live tumor cells cultured alone.

(B) Intercellular communication networks inferred by CellChat analysis between ADARreg^{high}-like (blue) or ADARreg^{low}-like (green) B cell and cytotoxic or inflammatory NK (red), or tumor-associated NK (TaNK) (brown), in ibrutinib slow responder CLL patient (CLL6).

(C) Gene expression at single–cell level of CLEC2D and ADARreg signature in B cells of fast (left) or slow (right) ibrutinib-responder CLL patients at pretreatment (pink), after 30 days (green), 120 days (blue), or 280 days (purple, slow responder patient only) of ibrutinib treatment.